Modification of the Stoner-Wohlfarth astroid by a spin-polarized current: An exact solution

Shu Yan,* Zhelin Sun,† and Ya. B. Bazaliy‡
Department of Physics and Astronomy, University of South Carolina, Columbia, South Carolina 29208
(Received 3 June 2013; published 12 August 2013)

The conventional Stoner-Wohlfarth astroid describes magnetic switching caused by an external magnetic field in a uniaxial, spatially uniform magnet. In spin-transfer devices the shape of the astroid is modified by the current-induced spin torque. The astroid shape modification is calculated here for a setup with the spin polarizer directed along the easy axis of the magnet, in which case the overall axial symmetry of the device is maintained. Our method does not rely on the assumption of small displacement of equilibria by the spin torque and takes into account that the destabilization of equilibrium states can be caused by two mechanisms: equilibrium merging, already active in a conventional astroid, and local equilibrium destabilization produced by the spin torque. The modified astroid has a self-crossing boundary and demonstrates a region with three stable equilibria. It is shown that the region of stable magnetic energy maximum can be reached only through a narrow bottleneck in the applied field space, which sets some stringent requirements for magnetic field alignment in the experiments. Switching diagrams are then calculated for the setups with magnetic field not perfectly aligned with the easy axis. Features not found in the approximate calculations are revealed and suggestions for their experimental observation are provided.

DOI: 10.1103/PhysRevB.88.054408 PACS number(s): 75.78.−n, 85.75.−d

I. INTRODUCTION

Studies of magnetic switching, i.e., of transitions between the distinct magnetic configurations have a long history. Since any device with reliable switching constitutes a potential magnetic memory cell, those investigations are often driven by the needs of applied disciplines. Nevertheless, they are also important in a fundamental sense allowing one to achieve a precise understanding of the switching mechanism.

For a long time the only available method of causing magnetic switching was an application of external magnetic field. In general, field-driven transitions between nonuniform magnetic configurations characterized by multiple magnetic domains require rather complicated theories for their description.[1] A simpler switching behavior is found in samples with spatially uniform magnetization, such as nanosize magnets with dimensions much smaller than the characteristic domain wall width. Here the switching is governed by the anisotropy energy and takes a particularly simple form in the case of an easy axis anisotropy. In this case the solution of the magnetic switching problems produces the "astroid" curve.[2]

Theoretical predictions of the spin-transfer torque made by Berger[3] and Slonczewski[4] opened a new possibility for magnetization control. If a spin-polarized current is injected into the magnet, an additional nonequilibrium torque is produced. This torque is proportional to the current magnitude and at sufficiently high currents it can switch the magnetization of a nanoparticle even in the absence of the external field.[4,6–9]

When both the field-induced torque and the spin torque are applied, the switching is a result of their combined action. The state of the nanomagnet is now controlled by two experimental parameters: the field and the current. One of the ways to understand this situation is to consider field switching at a fixed current magnitude. The solution to this problem gives the "modified astroid." Here we consider the spin torque modified astroids in the axially symmetric case with spin polarization of the current directed along the easy axis of the magnet. Experimentally this case is realized in spin valves using Co/Ni and/or Co/Pt multilayer stacks for their magnetic parts.[5] Such multilayers exhibit a strong interfacial anisotropy directed perpendicular to their planes and forcing the easy axis of the magnet and the current spin polarization to point along the nanowire (Fig. 1, upper panel). For spin valves of circular cross section the overall axial symmetry is thus maintained. Modification of the astroid in an axially symmetric case was studied by several authors, starting from the early numeric calculations.[10] Analytic approaches of subsequent studies[11–15] used certain approximations to get the astroid shape. Several related publications[16,17] considered the cases of more complicated anisotropies. In this paper we find the modified astroid in an exact fashion. Consistent application of the theory reproduces many previous results[11–15] but also shows important differences and additional features.

To formulate the problem more precisely we first briefly review the case of a conventional astroid. The states of the uniformly magnetized particle are fully characterized by a magnetization vector $\mathbf{M}$ with constant absolute value M_s so that $\mathbf{M} = \mathbf{m}M_s$, and $\mathbf{m}$ is a unit vector. Field-induced switching is completely controlled by the magnetic anisotropy and demagnetization energies. For the uniformly magnetized particles they add up to a total effective anisotropy energy $E_a(\mathbf{m})$. In a special case of uniaxial anisotropy one has

$$E_a = -K(\mathbf{m}\cdot\hat{z})^2, \tag{1}$$

where the unit vector $\hat{z}$ is chosen along the magnetic easy axis direction and K is the anisotropy constant. In the absence of external field the magnetization has two stable equilibrium directions, $\mathbf{m} = +\hat{z}$ and $\mathbf{m} = -\hat{z}$. When an external field $\mathbf{H}$ is applied and gradually increased in magnitude, the equilibria change their positions in response. Eventually one of them is destabilized, and a switching occurs at a critical field $\mathbf{H}_c$.

The collection of critical points $\mathbf{H}_c$ forms a "critical surface" S in the three-dimensional (3D) space of experimentally controlled parameters (H_x, H_y, H_z). When $\mathbf{H}$ approaches and

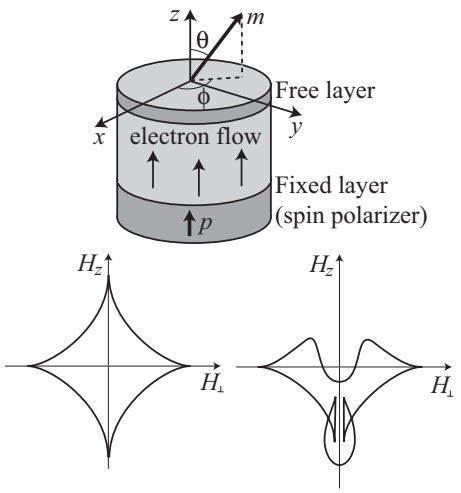

FIG. 1. (Upper panel) Spin torque device. Fixed magnetic layer creates the spin polarization of the current injected into the free magnetic layer. The easy axis of the free layer and the magnetization of the fixed layer are directed along the z axis. (Lower left) Conventional Stoner-Wholfarth astroid. (Lower right) Spin torque modified astroid with current directed so as to stabilize the $\mathbf{m} = +\hat{z}$ state (electrons flow from the fixed layer to the free layer). The features in the lower part of the astroid are exaggerated.

reaches S, one of the equilibria is destabilized. This equilibrium $\mathbf{m}_c$ will be called "critical." One can visualize $\mathbf{m}_c$ as a point on the unit sphere in the (m_x, m_y, m_z) space. This point changes its position in response to a change of applied field so that $\mathbf{m}_c = \mathbf{m}_c(\mathbf{H})$. If the applied field is slowly varied in time, and the system resides in the critical equilibrium, a jump to a different state will occur when the trajectory $\mathbf{H}(t)$ crosses S. Importantly, if $\mathbf{H}(t)$ later crosses the critical surface backwards at the same point, no switching will be observed, since now the system does not reside in the critical equilibrium. To sum up, every point of the critical surface S is characterized by a certain critical state $\mathbf{m}_c$, and the side of the surface on which this state is stable.

In the case of a uniaxial anisotropy, the axial symmetry of E_a with respect to the z axis leads to a corresponding symmetry of the critical surface: S becomes a figure of revolution around $\hat{z}$. One can therefore study a generatrix curve of S in the 2D plane $(H_\perp, H_z)$, where $H_\perp = \sqrt{H_x^2 + H_y^2}$. This critical curve is the Stoner-Wohlfarth astroid[2] shown in Fig. 1 (lower left).

In the presence of a spin-transfer torque magnetic switching is controlled by one additional parameter, the electric current I. We consider the case where the spin polarizer $\mathbf{p}$ is directed along $+\hat{z}$ (Fig. 1, upper panel). In such a setup the overall axial symmetry is preserved, S remains a figure of revolution in the H space, and the switching can be described by a surface in a 3D parameter space $(H_\perp, H_z, I)$. Modified astroids are the sections of this 3D surface by various $I = \text{const}$ planes. Jumping ahead, we show a sketch of a representative section found in this paper in Fig. 1 (lower right). The switching boundaries display a predictable overall shift towards the lower values of H_z: The sign of I is chosen so as to stabilize the $+\hat{z}$ state and destabilize the $-\hat{z}$ state. Naturally, less positive field H_z is required to destabilize the $-\hat{z}$ state, and a "depression" develops at the top of the astroid. Likewise, a larger negative H_z is required to destabilize the $+\hat{z}$ state, and a "bubble" develops at the bottom of the astroid. The bubble is connected to the main body of the modified astroid by a "bottleneck." The depression and the bubble were identified in Ref. 12, though in some form they were already found in Ref. 10. The elements of the figure suggested in this paper are the bottleneck and the self-crossing character of the boundary near it (Fig. 1, lower right). Their explanation is our first major result.

Plotting the $I = \text{const}$ sections is not the only possible way to visualize the critical surfaces in the 3D space $(H_\perp, H_z, I)$. Alternatively one could study the $H_\perp = \text{const}$ sections. A particular section with $H_\perp = 0$ was a subject of many investigations (see, e.g., Ref. 18 and references therein) and is well understood. This section describes the experiments conducted in an axial external field $\mathbf{H} = (0, 0, H_z)$. Of course, in practice the field cannot be aligned perfectly and a certain shift or angular misalignment can exist. Studies[14,15] that used the approximation of small equilibrium displacements found that even a small field misalignment produces qualitative changes in the switching diagram shape. Our exact analysis shows that the structure of the switching diagram is richer than predicted by the approximate calculations. We find that it is the narrowness of the bottleneck connecting the lower bubble to the main body of the astroid that allows small inaccuracies in the field alignment to produce significant qualitative changes in the picture of critical lines. We plot the switching diagrams and discuss their dependence on the field misalignment angle. This constitutes our second major result.

II. PROCEDURE FOR FINDING THE CRITICAL SURFACES

A. Magnetic dynamics in the presence of spin torques

The motion of magnetization $\mathbf{M}$ of the free layer is governed by the Landau-Lifshitz-Gilbert (LLG) equation either in its Gilbert form (we use the SI units),

$$\frac{d\mathbf{M}}{dt} = -\gamma\mu_0 \mathbf{M} \times \mathbf{H}_{\text{eff}} + \frac{\alpha}{M_s} \mathbf{M} \times \dot{\mathbf{M}}, \tag{2}$$

or in the Landau-Lifshitz form,

$$\frac{d\mathbf{M}}{dt} = -\frac{\gamma\mu_0}{1+\alpha^2} \mathbf{M} \times \mathbf{H}_{\text{eff}} - \frac{\gamma\mu_0\alpha}{(1+\alpha^2)M_s} \mathbf{M} \times (\mathbf{M} \times \mathbf{H}_{\text{eff}}), \tag{3}$$

where α is the Gilbert damping parameter and γ is the electron gyromagnetic ratio. The effective field $\mathbf{H}_{\text{eff}}$ accounts for (a) externally applied magnetic fields, (b) magnetic anisotropy, and (c) spin torques generated in spin transfer systems. It is a sum of three terms,

$$\mathbf{H}_{\text{eff}} = \mathbf{H} + \mathbf{H}_{\text{a}} + \mathbf{H}_{\text{st}}, \tag{4}$$

where $\mathbf{H}_{\text{a}}$ and $\mathbf{H}_{\text{st}}$ are the anisotropy field and the Slonczewski spin-transfer torque field,[4,9,19–22] respectively,

$$\mathbf{H}_{\text{a}} = -\frac{1}{\mu_0 M_s} \frac{\partial E_a}{\partial \mathbf{m}} = H_k m_z \hat{z}, \tag{5}$$

$$\mathbf{H}_{\text{st}} = \frac{1}{\mu_0 M_s} \frac{I}{Ae} \frac{\hbar}{2} \frac{1}{d}\, g(\mathbf{m} \cdot \hat{\mathbf{p}})(\mathbf{m} \times \hat{\mathbf{p}}) = \frac{1}{\mu_0 M_s} \frac{I}{Ae} \frac{\hbar}{2} \frac{1}{d}\, g(m_z)(\mathbf{m} \times \hat{z}). \tag{6}$$

Here $H_k = 2K/\mu_0 M_s$ is the anisotropy field, $I/Ae = j/e$ is the particle current density of itinerant electrons (with A being the cross-section area of the device and j being the electric current density), d is the thickness of the free layer, $g(\mathbf{m}\cdot\hat{\mathbf{p}})$ is the spin-torque efficiency function, and we have substituted $\mathbf{p} = +\hat{z}$. Our representative results will be obtained using the Slonczewski's function,[4,9]

$$g(\mathbf{m}\cdot\hat{\mathbf{p}}) = \frac{1}{(1+P)^3(3+\hat{\mathbf{m}}\cdot\hat{\mathbf{p}})/4P^{3/2} - 4}, \tag{7}$$

where P is the degree of electron spin polarization in the ferromagnetic material of the free and fixed layers.

Equation (3) can be rewritten in standard spherical coordinates (θ,ϕ) associated with the unit vector $\mathbf{m} = (\sin\theta\cos\phi, \sin\theta\sin\phi, \cos\theta)$ (Fig. 1, upper panel). Using three orthogonal unit vectors $\mathbf{m}$, $\mathbf{e}_\theta = \partial\hat{\mathbf{m}}/\partial\theta$ and $\mathbf{e}_\phi = (1/\sin\theta)\partial\hat{\mathbf{m}}/\partial\phi$, and absorbing $\gamma\mu_0 H_k$ into the redefinition of time we get

$$\begin{aligned}(1+\alpha^2)\dot{\theta} &= \mathbf{h}_{\rm eff}\cdot\mathbf{e}_\phi + \alpha\mathbf{h}_{\rm eff}\cdot\mathbf{e}_\theta,\\ (1+\alpha^2)\sin\theta\,\dot{\phi} &= -\mathbf{h}_{\rm eff}\cdot\mathbf{e}_\theta + \alpha\mathbf{h}_{\rm eff}\cdot\mathbf{e}_\phi,\end{aligned} \tag{8}$$

where the normalized field is $\mathbf{h}_{\rm eff} = \mathbf{H}_{\rm eff}/H_k$. At equilibrium, both θ and ϕ should be time independent. In our case this leads to a system of equations,

$$(h_{\rm eff})^\theta \equiv \mathbf{h}_{\rm eff}\cdot\mathbf{e}_\theta = -\frac{\partial\varepsilon}{\partial\theta} + \mathbf{h}\cdot\mathbf{e}_\theta = 0, \tag{9a}$$

$$(h_{\rm eff})^\phi \equiv \mathbf{h}_{\rm eff}\cdot\mathbf{e}_\phi = \mathbf{h}\cdot\mathbf{e}_\phi + h_{\rm st} = 0. \tag{9b}$$

Here

$$\varepsilon(\theta) = \frac{E_a}{\mu_0 M_s H_k} = -\frac{1}{2}\cos^2\theta \tag{10}$$

is the rescaled dimensionless anisotropy energy (from now on we drop the subscript "a" for convenience of notation). For $\mathbf{p} = +\hat{z}$ the spin torque field is directed along $\mathbf{e}_\phi$. Thus it does not appear in Eq. (9a) and contributes a term,

$$h_{\rm st}(\theta, j) = \frac{\mathbf{H}_{\rm st}\cdot\mathbf{e}_\phi}{H_k} = -\frac{j}{j_0}g(\cos\theta)\sin\theta, \tag{11}$$

to Eq. (9b) with the characteristic current density defined as $j_0 = 4edK/\hbar$ (we use j instead of I in the following calculations). The spin torque term h_{st} is proportional to the current and vanishes at $j = 0$.

B. Equilibrium states

Normally one would like to solve Eqs. (9a) and (9b) and find the equilibrium angles (θ_0,ϕ_0) as functions of the parameters $\mathbf{h}$ and j. This way one would get all equilibria $\mathbf{m}_{0i}(\mathbf{h}, j)$ for a given set of experimental parameters (index i reflects the existence of multiple equilibria). After that one can study the stability of those equilibria in order to find the critical surface S. However, as shown in Ref. 23 it is easier to search for the critical surface using a variation of the method of Lagrange multipliers. Namely, we will solve the system backwards, assuming (θ_0,ϕ_0) to be given, and searching for an external field $\mathbf{h}$ which makes $\mathbf{m}_0$ an equilibrium at a given current. It is easy to see from the system (8) that such an $\mathbf{h}$ is not unique: If a particular field $\mathbf{h}_0$ solves the equilibrium equations, then the field $\mathbf{h} = \mathbf{h}_0 + \lambda\mathbf{m}_0$ with arbitrary λ will also be a solution. Solutions for given $\mathbf{m}_0$ and j fill a whole line in the h space. We will call it a "λ line." Using (9a) and (9b) we find the λ line equation,

$$\mathbf{h}(\mathbf{m}_0, j, \lambda) = \frac{\partial\varepsilon}{\partial\theta}\mathbf{e}_\theta(\mathbf{m}_0) - h_{\rm st}\mathbf{e}_\phi(\mathbf{m}_0) + \lambda\mathbf{m}_0. \tag{12}$$

Note that the first two terms in this expression are orthogonal to $\mathbf{m}_0$. Equation (12) defines a mapping of vectors $\mathbf{m}_0$ residing on a two-dimensional (2D) unit sphere to the 3D h space. Alternatively it can be viewed as a mapping from a 3D $(\mathbf{m}_0,\lambda)$ space to the h space.

C. Stability of equilibria

While $\mathbf{m}_0$ is an equilibrium everywhere on the λ line, it is not necessarily always a stable equilibrium. Let us study the stability of $\mathbf{m}_0$ in an applied field $\mathbf{h}$ given by Eq. (12) with a certain value of λ. To do that we investigate the linear expansion of Eq. (8) up to the first order in deviations of $\mathbf{m}$ from the equilibrium. The deviations are characterized by the angle increments $(\delta\theta,\delta\phi)$. Of course, in this expansion only $\mathbf{m}$ is varied and $\mathbf{h}(\mathbf{m}_0, j, \lambda)$ remains constant. Linear expansion provides a system of two coupled linear differential equations,

$$\begin{pmatrix}\dot{\delta\theta}\\ \sin\theta_0\dot{\delta\phi}\end{pmatrix} = \mathbf{D}\begin{pmatrix}\delta\theta\\ \sin\theta_0\delta\phi\end{pmatrix}, \tag{13}$$

where $\mathbf{D}(\mathbf{m}_0, j, \lambda)$ is a 2×2 matrix,

$$\mathbf{D} = \frac{1}{1+\alpha^2}\begin{pmatrix}\partial f^\theta/\partial\theta & (\partial f^\theta/\partial\phi)/\sin\theta\\ \partial f^\phi/\partial\theta & (\partial f^\phi/\partial\phi)/\sin\theta\end{pmatrix}\Bigg|_{\theta_0,\phi_0}, \tag{14}$$

with

$$f^\theta = {h_{\rm eff}}^\phi + \alpha {h_{\rm eff}}^\theta, \quad f^\phi = -{h_{\rm eff}}^\theta + \alpha {h_{\rm eff}}^\phi.$$

Stability of an equilibrium requires both eigenvalues $\mu_{1,2}$ of the matrix $\mathbf{D}(\mathbf{m}_0, j, \lambda)$ to have negative real parts. In the case of a 2×2 matrix,

$$\mu_{1,2} = \frac{\rm tr[\mathbf{D}]}{2} \pm \sqrt{\left(\frac{\rm tr[\mathbf{D}]}{2}\right)^2 - \det[\mathbf{D}]}, \tag{15}$$

and the ${\rm Re}[\mu_{1,2}] < 0$ requirement is equivalent to two inequalities: $\det[\mathbf{D}] > 0$ and ${\rm tr}[\mathbf{D}] < 0$. Accordingly, an equilibrium will be destabilized if either the determinant or the trace change their signs. The determinant and the trace of $\mathbf{D}(\mathbf{m}_0, j, \lambda)$ are given by the expressions (for brevity we drop the subscript "0" in the equilibrium angles θ_0 and ϕ_0),

$$\det[\mathbf{D}] = \frac{1}{1+\alpha^2}\frac{1}{\sin\theta}\left(\frac{\partial {h_{\rm eff}}^\theta}{\partial\theta}\frac{\partial {h_{\rm eff}}^\phi}{\partial\phi} - \frac{\partial {h_{\rm eff}}^\phi}{\partial\theta}\frac{\partial {h_{\rm eff}}^\theta}{\partial\phi}\right), \tag{16}$$

and

$$\begin{aligned}{\rm tr}[\mathbf{D}] = \frac{1}{1+\alpha^2}\Bigg[&\frac{\partial {h_{\rm eff}}^\phi}{\partial\theta} - \frac{1}{\sin\theta}\frac{\partial {h_{\rm eff}}^\theta}{\partial\phi}\\ &+\alpha\left(\frac{\partial {h_{\rm eff}}^\theta}{\partial\theta} + \frac{1}{\sin\theta}\frac{\partial {h_{\rm eff}}^\phi}{\partial\phi}\right)\Bigg].\end{aligned} \tag{17}$$

Whenever we will study the trace and the determinant on a given λ line, a shortened notation $\mathbf{D}(\lambda)$ will be used. Substituting Eqs. (9a), (9b), and (12) into (16), we find that

the determinant is a quadratic function of λ with a positive coefficient at the λ^2 term. For $\varepsilon = \varepsilon(\theta)$ and $\mathbf{p} = +\hat{z}$ the two roots of the equation $\det[\mathbf{D}(\lambda)] = 0$ are given by

$$\lambda_\pm = -\frac{1}{2\sin\theta}\frac{\partial(\sin\theta\varepsilon'_\theta)}{\partial\theta} \pm \sqrt{\frac{1}{4}\left(\varepsilon''_{\theta\theta} - \frac{\cos\theta}{\sin\theta}\varepsilon'_\theta\right)^2 - \Delta}.$$

Here ε'_θ stands for $\partial\varepsilon/\partial\theta$, etc.; Δ contains all the spin-torque terms and is given by

$$\Delta = \frac{\cos\theta}{\sin\theta}\, h_{\rm st}\frac{\partial h_{\rm st}}{\partial\theta}.$$

Substituting ε from (10) we get

$$\lambda_\pm = \frac{1}{2}\sin^2\theta - \cos^2\theta \pm \sqrt{\frac{1}{4}\sin^4\theta - \frac{\cos\theta}{\sin\theta}h_{\rm st}\frac{\partial h_{\rm st}}{\partial\theta}}. \quad (18)$$

Next, a substitution of Eqs. (9a), (9b), and (12) into (17) shows that the trace is a linear function of λ with a negative slope and the root of the equation $\mathrm{tr}\mathbf{D}(\lambda) = 0$ is given by

$$\begin{aligned}\lambda_{\rm T} &= -\frac{1}{2\sin\theta}\frac{\partial}{\partial\theta}\left[\sin\theta\left(\varepsilon'_\theta - \frac{h_{\rm st}}{\alpha}\right)\right] \\ &= \frac{1}{2}\sin^2\theta - \cos^2\theta + \frac{1}{2\alpha}\left(\frac{\cos\theta}{\sin\theta}h_{\rm st} + \frac{\partial h_{\rm st}}{\partial\theta}\right). \quad (19)\end{aligned}$$

Two situations are possible:

(1) The roots $\lambda_\pm$ are real. Then for λ outside of the interval (λ_-,λ_+) the equilibrium is a focus or a node in the sense of the dynamical systems theory (Appendix A). It is stable for $\lambda > \lambda_{\rm T}$ and unstable otherwise. For λ inside the (λ_-,λ_+) interval the equilibrium is a saddle point, which is always unstable. The stability condition takes the form,

$$\begin{gathered}\lambda > \lambda_{\rm T} \quad \text{and} \quad \lambda < \lambda_-, \\ \text{or} \\ \lambda > \lambda_{\rm T} \quad \text{and} \quad \lambda > \lambda_+. \end{gathered} \quad (20)$$

(2) There are no real roots of $\det[\mathbf{D}] = 0$, i.e., $\lambda_\pm$ are complex conjugate numbers. Then the determinant condition is satisfied for any λ, and the equilibrium is always a focus or a node. Stability condition takes a form,

$$\lambda > \lambda_{\rm T} \quad \text{and} \quad \mathrm{Im}[\lambda_\pm] \neq 0. \quad (21)$$

In the absence of spin-polarized current one gets $\Delta = 0$, both λ_+ and λ_- are real, and $\lambda_{\rm T} = (\lambda_+ + \lambda_-)/2$. Stability condition (20) is satisfied for $\lambda \in (\lambda_+,\infty)$, i.e., $\mathbf{m}_0$ is stable when $\mathbf{h}$ belongs to a semi-infinite ray in the h space. In the presence of current, more complicated divisions of the λ line into stable and unstable intervals can occur. For example, if $\lambda_\pm$ are real and $\lambda_{\rm T} < \lambda_-$, there will be two intervals of stability: $(\lambda_{\rm T},\lambda_-)$ and (λ_+,∞).

Note that the current-dependent term in the expression (19) comes with a factor of $1/\alpha$. Since Gilbert damping is small, this means that $\lambda_{\rm T}$ is very sensitive to the changes of the current. The term Δ, representing the current contribution to Eq. (18), does not contain a similar large factor, thus $\lambda_\pm$ are relatively insensitive to the current changes.

D. Critical surfaces

We have shown that each λ line is divided into the intervals of stability and instability of $\mathbf{m}_0$, and the end points of these intervals are given by

$$\mathbf{h}_\pm = \mathbf{h}(\mathbf{m}_0, j, \lambda_\pm(\mathbf{m}_0, j)), \quad \mathbf{h}_{\rm T} = \mathbf{h}(\mathbf{m}_0, j, \lambda_{\rm T}(\mathbf{m}_0, j)), \quad (22)$$

with the right-hand sides specified by Eq. (12). It was shown in Ref. 23 that the sets of points $\mathbf{h}_\pm(\mathbf{m}_0)$,$\mathbf{h}_{\rm T}(\mathbf{m}_0)$, obtained as the argument $\mathbf{m}_0$ runs through all of its possible values, form the three sheets S_+, S_-, $S_{\rm T}$ of the critical surface S. Therefore one may view the subscript "c" in the critical field $\mathbf{h}_c$ as an index assuming the values of "+", "−", or "T". In the most general case all three sheets of S are relevant. However, there are special cases, e.g., the above-mentioned case of zero current with $\lambda_- < \lambda_{\rm T} < \lambda_+$, where some of the sheets become irrelevant and are not included into S.

Note that this procedure produces the critical surface, but does not yet provide complete information about switching. Namely, it does not explicitly show which side of the surface corresponds to the stability of $\mathbf{m}_0$. Such an analysis has to be performed additionally, after the critical surface is found.

III. MODIFICATION OF THE STONER-WOHLFARTH ASTROID

The critical surface sheets (22) of the modified astroid are obtained by substituting expressions (18) and (19) into Eq. (12). The resulting formulas are exact but very long. Representative astroid shapes shown in the figures in this section were obtained for spin polarization $P = 0.5$ and current magnitude $j/j_0 = \alpha = 0.1$. Some of the figures show sketches that are not drawn to scale but instead emphasize the features produced by the spin torque.

A. Conventional Stoner-Wohlfarth astroid

First we consider the case of $j = 0$ to illustrate the method by reproducing the conventional astroid. With $h_{st} = 0$ and axially symmetric energy $\varepsilon(\theta)$ Eqs. (12) and (22) specialize to

$$\mathbf{h}_c(\mathbf{m}_0) = \frac{\partial\varepsilon}{\partial\theta}\mathbf{e}_\theta(\mathbf{m}_0) + \lambda_c(\mathbf{m}_0)\mathbf{m}_0. \quad (23)$$

One can see that $\mathbf{h}_c$ lies in the plane formed by the vectors $\mathbf{m}_0$ and $\hat{z}$. Together with the fact that the critical surface is a figure of revolution this means that if $\mathbf{m}_0$ is varied in any $\phi = \mathrm{const}$ plane, then the points $\mathbf{h}_c(\mathbf{m}_0)$ form the entire generatrix of S, i.e., the desired critical curve in the $(h_\perp,h_z)$ plane. In practice we set $\phi = 0$ and obtain the $(h_{c\perp}(\theta),h_{cz}(\theta)) = (h_{cx}(\theta),h_{cz}(\theta))$ critical curve by varying θ in the $[0,\pi]$ interval. Three functions $\lambda_c(\theta)$ ($c = +, -, \mathrm{T}$) are shown in Fig. 2 (left). At $j = 0$ the value of $\lambda_{\rm T}$ lies between the two real values λ_+ and λ_- (see Sec. II C). Therefore there is only one boundary, $\lambda_+(\theta)$, separating the stable and the unstable regions. Critical curves $\mathbf{h}_c(\theta)$ are plotted in Fig. 3 (left). Only the $\mathbf{h}_+(\theta)$ curve is relevant and it reproduces the conventional astroid.

The states destabilized at each point of S_+ are well known. For a field inside the astroid there are four equilibrium states: An energy minimum $\mathbf{m}_{\rm min}^{(+)}$ in the upper hemisphere, another minimum $\mathbf{m}_{\rm min}^{(-)}$ in the lower hemisphere, a maximum $\mathbf{m}_{\rm max}$, and a saddle point $\mathbf{m}_{\rm sdl}$. When $\mathbf{h}$ reaches the astroid boundary from inside, one of the minima collides with a saddle point and disappears.

A comment has to be made about the relationship between Fig. 2 (left) and Fig. 3 (left). In the mapping [(Eqs. (12)

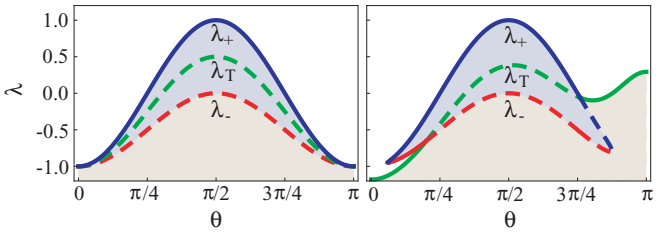

FIG. 2. (Color online) The $\lambda_+(\theta)$, $\lambda_-(\theta)$, and $\lambda_T(\theta)$ curves shown by black (blue), gray (red), and light gray (green) curves, respectively. The relevant parts of the curves are shown as solid and irrelevant as dashed lines. The stable region is shown in white. (Left panel) $j = 0$ conventional case. Stable region is given by $\lambda > \lambda_+$. (Right panel) $j = 0.1\,j_0$. In the presence of spin torque the stable region is given by the conditions (20) and (21).

and (22)] the $\lambda_c(\theta)$ curves are mapped one-to-one to the $\mathbf{h}_c(\theta)$ curves. However, the mapping of the stability region $\lambda > \lambda_+(\theta)$ shown in white in Fig. 2 (left) is more complicated. This region is mapped on the whole h plane in such a way that each $(h_\perp,h_z)$ point outside the astroid has one stable equilibrium point (θ,λ) mapped to it, and each point inside the astroid has two stable points mapped to it.

B. Modified astroid

The case of a nonzero current $j \neq 0$ has two important differences from the conventional case. First, according to Eqs. (12) and (22) the $\mathbf{h}_c(\mathbf{m}_0)$ vectors are not necessary lying in the plane formed by $\mathbf{m}_0$ and $\hat{z}$. Second, more than one point $\mathbf{h}_c(\mathbf{m}_0)$ may be relevant on some λ lines.

The first circumstance means that for $\mathbf{m}_0$ characterized by $\phi = 0$ all three components of the critical field $\mathbf{h}_c(\mathbf{m}_0)$ will be nonzero. However, due to the axial symmetry of the problem the relative orientation of the vectors $\mathbf{m}_0$, $\hat{z}$, and $\mathbf{h}_c(\mathbf{m}_0)$ is the same regardless of ϕ, and S remains a figure of revolution. It is therefore still sufficient to consider a subset of vectors $\mathbf{m}_0$ characterized by a fixed $\phi = 0$ and variable $\theta \in [0,\pi]$ to obtain the entire generatrix of the critical surface given by $(h_{c\perp}(\theta),h_{cz}(\theta)) = (\sqrt{h_{cx}^2(\theta) + h_{cy}^2(\theta)}\,,h_{cz}(\theta))$.

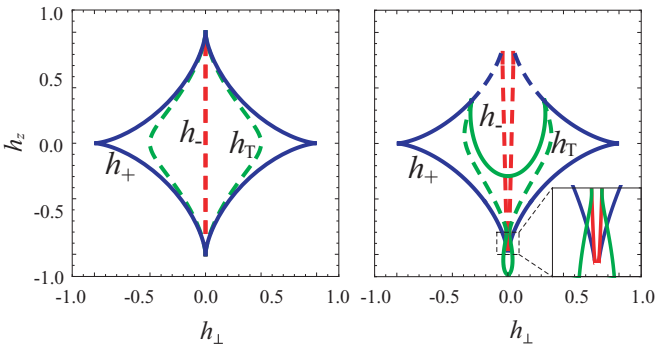

FIG. 3. (Color online) Stoner-Wohlfarth astroids. (Left panel) $j = 0$; (right panel) $j = 0.1\,j_0$. Critical field curves $\mathbf{h}_c$ are shown using the same convention as in Fig. 2 above. The astroids are formed by the images of the relevant (solid) parts of the λ_c curves from that figure.

The second circumstance reflects the main qualitative difference between the scenarios possible in conventional and spin torque switching.[25] For $j = 0$ the destabilization of an equilibrium can only happen due to the sign change of det[**D**]. As a result, stable equilibria do not just become unstable upon crossing the astroid boundary but disappear altogether in the process of merging with other equilibria. For $j \neq 0$ an additional scenario is possible in which the spin torque changes the sign of tr[**D**], enabling a local destabilization of an equilibrium. Locally destabilized equilibria still exist on the other side of the critical surface but are unstable and do not show up in experiments.

The functions $\lambda_\pm(\theta)$ and $\lambda_T(\theta)$ at $j \neq 0$ are plotted in Fig. 2 (right). One can see that every arrangement of $\lambda_\pm$ and λ_T discussed in Sec. II C can be found for an appropriate value of θ. An application of the criteria (20) and (21) gives the region of stability shown as a white area. The boundary of the stability region is composed of the pieces of $\lambda_\pm$ and λ_T curves. The corresponding pieces of the $\mathbf{h}_\pm$ and $\mathbf{h}_T$ curves constitute the modified astroid (Fig. 3, right), which exhibits the features announced in Fig. 1 (lower right). The inset to Fig. 3 (right) shows an enlarged view of the bubble in the lower part of the astroid. One can see the bottleneck that connects the bubble to the main body of the astroid and the triangular regions formed by the self-crossing boundary. The details of these features will be discussed below.

C. Analysis of equilibria and destabilization modes

As explained in Sec. II D, we now have to identify which side of S corresponds to a stable critical equilibrium and describe these equilibria at every point of S. A remark about the nature of equilibria in the presence of spin torque is due here. For $j = 0$ the equilibria coincide with the extremum points of the total magnetic energy $\varepsilon_{\rm tot} = \varepsilon(\mathbf{m}) - \mathbf{h}\cdot\mathbf{m}$. The energy minima are always stable, the energy maxima and the saddle points are always unstable. For $j \neq 0$ the equilibria are not located in the extrema of $\varepsilon_{\rm tot}$ and cannot be classified this way. One can prove that the spin-transfer torque field cannot be represented as $\mathbf{h}_{st} = \partial\varepsilon_{\rm st}/\partial\mathbf{m}$ by some energy function $\varepsilon_{\rm st}$,[18] and no effective energy of the type $\varepsilon_{\rm eff} = \varepsilon_{\rm tot} + \varepsilon_{\rm st}$ can be defined. Nevertheless, it is frequently stated in the literature that the spin torque can "destabilize an energy minimum" or "stabilize an energy maximum." Such statements cannot be precise unless one defines when an equilibrium should be called a minimum or a maximum in the $j \neq 0$ situation. As explained in Appendix A, it is the foci with a counterclockwise rotation of the torque field around them that should be identified as the quasiminima and the foci with a clockwise rotation—as the quasimaxima. In the text below we will drop the prefix "quasi" whenever it does not lead to a confusion. In the $j = 0$ case the stability of a focus and its rotation direction are linked to each other. This link is broken for $j \neq 0$, e.g., a quasimaximum can be unstable or stable depending on the current magnitude. The node-type equilibria cannot be meaningfully identified as either quasiminima or quasimaxima. The saddle points are unstable in both $j = 0$ and $j \neq 0$ cases.

It is worth noting here that the absence of an energy function describing the dynamics of the free layer in the presence of spin torque is not in contradiction with the notion of an effective

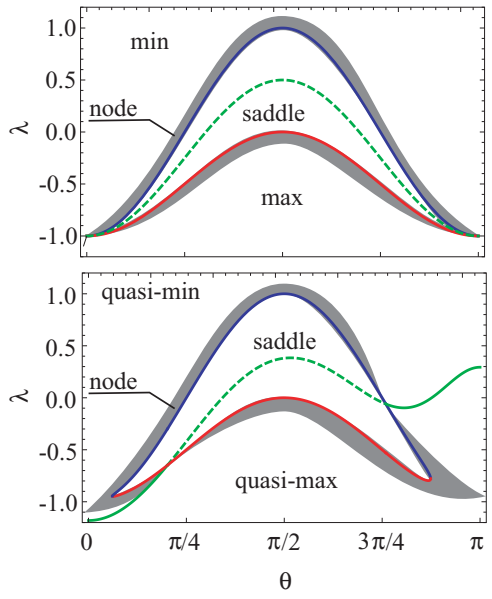

FIG. 4. (Color online) Separation of the (θ,λ) plane into the regions with different types of equilibria. The λ_c lines are shown using the convention of Fig. 2. (Upper panel) $j = 0$. (Lower panel) $j = 0.1 j_0$. The gray regions (drawn not to scale) containing the node-type equilibria are defined by the λ_f curves. One can prove that the width of this region reduces to zero at the intersections of the $\lambda_\pm$ and λ_T curves.

potential describing the behavior of spin transfer devices at finite temperatures.[26–31] That effective potential is not used in the LLG equation but is obtained by averaging the spin torque contribution over the unperturbed trajectories. Its functional form and the degree of applicability can be discussed only after the equilibrium points and the phase portrait of the system are understood in the LLG framework.

Each point of the (θ,λ) plane corresponds to an equilibrium state. Figure 4 shows a division of this plane into the regions of different types of equilibria. The gray area of node-type equilibria is bound by the curves $\lambda_f(\theta)$ on which the foci are converted into the nodes. According to Eq. (15) these curves can be obtained from an equation $\mathrm{tr}[\mathbf{D}(\lambda_f)]^2 - 4\det[\mathbf{D}(\lambda_f)] = 0$. As expected from the arguments given in Appendix A, the regions of foci with opposite senses of rotation have no common boundaries. In the $j = 0$ case (upper panel) they are separated by both the regions of nodes and saddle points. For $j \neq 0$ (lower panel) they are sometimes separated only by a band of node-type equilibria. In addition, in the $j \neq 0$ case the λ_T line separates the quasiminimum and quasimaximum areas into stable and unstable parts.

We now return to the question of finding the side of S where the critical equilibria are stable. The answer to it can be obtained from the mapping of the (θ,λ) plane on the $(h_\perp,h_z)$ plane defined by the formulas (12) and (22). Similar to the case of a conventional astroid, this is not a one-to-one mapping. To study it we return to Eqs. (9a) and (9b) and search for the equilibria $\mathbf{m}_0$ at a given applied field $\mathbf{h}$. If the field is chosen in the (x,z) plane, $\mathbf{h} = (h_x,0,h_z)$, the equilibrium $\mathbf{m}_0$ is characterized by the angles (ϕ,θ) with $\phi \neq 0$ due to the presence of spin torque. Explicitly calculating $\mathbf{h}\cdot\mathbf{e}_\theta = h_x\cos\theta\cos\phi - h_z\sin\theta$ and $\mathbf{h}\cdot\mathbf{e}_\phi = -h_x\sin\phi$, we

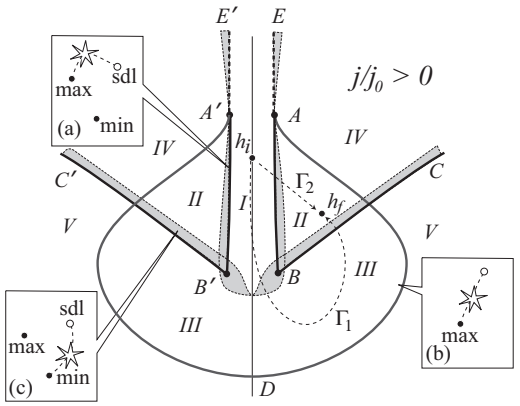

FIG. 5. Qualitative picture (drawn not to scale) of destabilization near the bottleneck. The equilibria in regions I, II, ... V are explained in the text. Upon entering into the gray band, one of the foci becomes a node. The insets show the destabilization scenarios on the critical surface. Trajectories Γ_1 and Γ_2 are discussed in the text to illustrate the dependence of the final state on the path taken.

get a system of equations:

$$\begin{aligned} -\sin\theta\cos\theta + h_x\cos\theta\cos\phi - h_z\sin\theta &= 0, \\ -h_x\sin\phi + h_{st}(\theta) &= 0. \end{aligned} \tag{24}$$

Its solutions were studied using a procedure described in Appendix B, and the results are summarized in Fig. 5. The equilibria are labeled in the same way as in Sec. III A: This turns out to be possible because in the axially symmetric case the spin torque does not create any new equilibria in comparison with the case of zero current.

The region of the $(h_\perp,h_z)$ plane shown in Fig. 5 corresponds to $h_z < 0$, so $\mathbf{m}_{min}^{(-)}$ is always stable and does not switch. We will be only interested in the evolution of $\mathbf{m}_{\mathrm{min}}^{(+)}$, $\mathbf{m}_{\mathrm{sdl}}$, and $\mathbf{m}_{\mathrm{max}}$. Let us start the discussion with region IV. When $\mathbf{h}$ resides in this region, the four equilibria have the same properties as they do at zero current inside a conventional astroid. Next, we slowly change the applied field, so that the point $\mathbf{h}(t)$ moves along a certain trajectory Γ in the $(h_\perp,h_z)$ plane. If Γ goes from region IV to region V, $\mathbf{m}_{\mathrm{min}}^{(+)}$ is annihilated in a collision with $\mathbf{m}_{\mathrm{sdl}}$ on the BC curve. Just before this collision $\mathbf{m}_{\mathrm{min}}^{(+)}$ enters the narrow gray band where its nature changes from a stable minimum to a stable node. Region V has two equilibria: a stable minimum $\mathbf{m}_{\mathrm{min}}^{(-)}$ and an unstable maximum $\mathbf{m}_{\mathrm{max}}$.

On a trajectory going from region IV to region II the maximum $\mathbf{m}_{\mathrm{max}}$ becomes a stable equilibrium on the ADA' curve. Stabilization of a maximum point by the spin torque is well known for an applied field of fixed direction.[4,7,18,24,25] The bubble bounded by the curve ADA' is the generalization of the stable maximum region for the case of variable field direction. Region II has four equilibria, of which three are stable ($\mathbf{m}_{\mathrm{min}}^{(-)}$, $\mathbf{m}_{\mathrm{min}}^{(+)}$, $\mathbf{m}_{\mathrm{max}}$), and one is unstable ($\mathbf{m}_{\mathrm{sdl}}$). In most of the region $\mathbf{m}_{\mathrm{min}}^{(-)}$ and $\mathbf{m}_{\mathrm{min}}^{(+)}$ are stable minima, and $\mathbf{m}_{\mathrm{max}}$ is a stable maximum. Inside the narrow gray bands one or more of the stable equilibria become stable nodes and strictly speaking cannot be called a quasimaximum or a quasiminimum. However, the narrowness of the gray bands makes it possible to loosely speak about region II as having two stable minima and one stable maximum. Node areas are

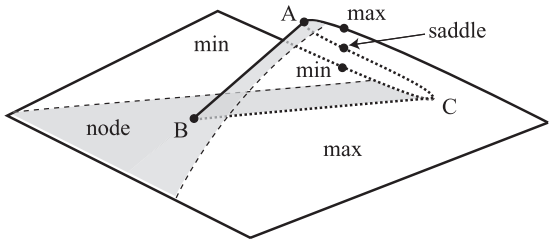

FIG. 6. The folding mapping (drawn not to scale) of the (θ,λ) plane to the $(h_\perp,h_z)$ plane in the vicinity of point B.

present in other regions as well. Whenever a loose description of the type discussed above is possible, we will not specifically mention them. However, sometimes the process of conversion of a minimum or a maximum into a node plays an essential role, e.g., when going from region I to region II. In those cases it will be discussed in detail.

The evolution of the equilibria on a trajectory going from region II into region III is similar to that on a trajectory going from IV to V. The $\mathbf{m}_{\min}^{(+)}$ state collides with $\mathbf{m}_{\rm sdl}$ on BC. The difference is that here $\mathbf{m}_{\max}$ is stable in II and remains stable in III. Altogether, region III has two stable equilibria: $\mathbf{m}_{\min}^{(-)}$ and $\mathbf{m}_{\max}$.

On a trajectory going from region II into region I a collision of $\mathbf{m}_{\max}$ and $\mathbf{m}_{\rm sdl}$ happens on the AB curve. Since $\mathbf{m}_{\max}$ is stable in II, this may produce an experimentally observable switching event. Region I has only two equilibria, both of which are stable minima $\mathbf{m}_{\min}^{(\pm)}$. A similar collision of $\mathbf{m}_{\max}$ with $\mathbf{m}_{\rm sdl}$ occurs upon going from region IV to region I across the AE boundary. But in contrast with the II $\rightarrow$ I transition, the maximum is already unstable in region IV and this collision does not produce a switching event: The AE boundary is irrelevant for switching and therefore is shown as a dashed line in Fig. 3 (right) and Fig. 5. It is interesting that the spin torque creates a distinct region I which does not exist at zero current. Inside this narrow "inner tube" around the z axis there are no saddle and maximum equilibria, and the pattern of torque field is qualitatively the same as in the case of $\mathbf{h}$ being exactly parallel to z.

It is instructive to consider an experiment with the field changing along the trajectories Γ_1 and Γ_2 shown in Fig. 5. These trajectories start with the system in the energy minimum state $\mathbf{m}_{\min}^{(+)}$ and reach the same final point in the h space. When the Γ_2 trajectory is followed, the system remains in the $\mathbf{m}_{\min}^{(+)}$ state: Crossing the AB curve does not affect $\mathbf{m}_{\min}^{(+)}$ because, as discussed above, this equilibrium is not critical on AB. In contrast, following Γ_1 brings the system into the $\mathbf{m}_{\max}$ state. On this trajectory the equilibrium experiences transformations while crossing the gray band of node-type equilibria. Upon entering this band the minimum $\mathbf{m}_{\min}^{(+)}$ is converted into a stable node, and upon exiting the band on the other side it is further converted into a stable focus with an opposite sense of rotation, i.e., into a stable maximum $\mathbf{m}_{\max}$. Regions I and III both have two stable equilibria, one of them being $\mathbf{m}_{\min}^{(-)}$, and the other being a stable minimum $\mathbf{m}_{\min}^{(+)}$ in region I and a stable maximum $\mathbf{m}_{\max}$ in region III.

The behavior of equilibria described above can be summarized by a picture of the $(\theta,\lambda) \rightarrow (h_\perp,h_z)$ mapping in the vicinity of point B (Fig. 6). This mapping folds the (θ,λ) plane into three sheets on the right of the point B, while on the left of B the plane remains unfolded. One can see by inspection that in the vicinity of B such a procedure transforms the regions of the equilibria shown in Fig. 4 into the regions shown in Fig. 5. In the folded region the minima reside on the lower sheet, the maxima on the upper sheet, and the saddle points occupy the middle sheet. A trajectory going on the right of B (e.g., the Γ_2 trajectory in Fig. 5) remains on the lower sheet until it hits the BC curve where the minimum collides with the saddle. A trajectory going on the left of B (e.g., the Γ_1 trajectory in Fig. 5) climbs to the top sheet. This trajectory does not intersect with the BC curve since the two belong to different sheets of the surface. As the field moves along Γ_1, the equilibrium is converted form a minimum to a maximum after it crosses the gray band. If such a trajectory eventually reaches the AB curve, the maximum collides with the saddle and disappears.

IV. SWITCHING DIAGRAMS IN A SLIGHTLY MISALIGNED AXIAL FIELD

The presence of a narrow bottleneck in the modified astroid means that although the bubble region may be reasonably large, it is rather hard to reach the stable maximum state inside of it by varying the external field. Consider an experiment where the applied field is nominally directed along the easy axis but in reality is slightly misaligned.[11,13–15] A field with a tilt angle β with respect to $\hat{z}$ evolves along a trajectory Γ_β given by a straight line $(h_\perp,h_z) = (h\sin\beta, h\cos\beta)$ (Fig. 7). The system starting from the $\mathbf{m}_{\min}^{(+)}$ state at zero applied field will evolve into the stable maximum only if Γ_β is kept inside the bottleneck (trajectory $\Gamma_{\beta 1}$). If the trajectory wanders outside of the bottleneck and the BC line is crossed (trajectory $\Gamma_{\beta 2}$), the stable minimum collides with the saddle point and is never converted into a stable maximum. The width of the bottleneck Δh can be estimated in the limit $j/j_0 \ll 1$ where we have obtained

$$\begin{aligned} \Delta h &\approx 4\left(g|_{\theta=0}\frac{j}{j_0}\right)^{3/2} \quad (j/j_0 > 0), \\ \Delta h &\approx 4\left(g|_{\theta=\pi}\frac{j}{j_0}\right)^{3/2} \quad (j/j_0 < 0). \end{aligned} \tag{25}$$

For $j/j_0 = 0.1$ and $P = 50\%$ this approximation gives $\Delta h = 9.71 \times 10^{-3}$ in good agreement with the actual bottleneck width $\Delta h = 9.68 \times 10^{-3}$ found in Fig. 3 (right).

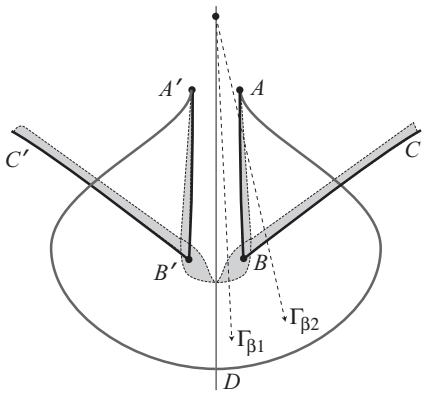

FIG. 7. Trajectories $\Gamma_{\beta 1}$ and $\Gamma_{\beta 2}$ (drawn not to scale) represent two tilting angles of the applied field. Both of them lead into the bubble region but the stable maximum state is reached only along $\Gamma_{\beta 1}$.

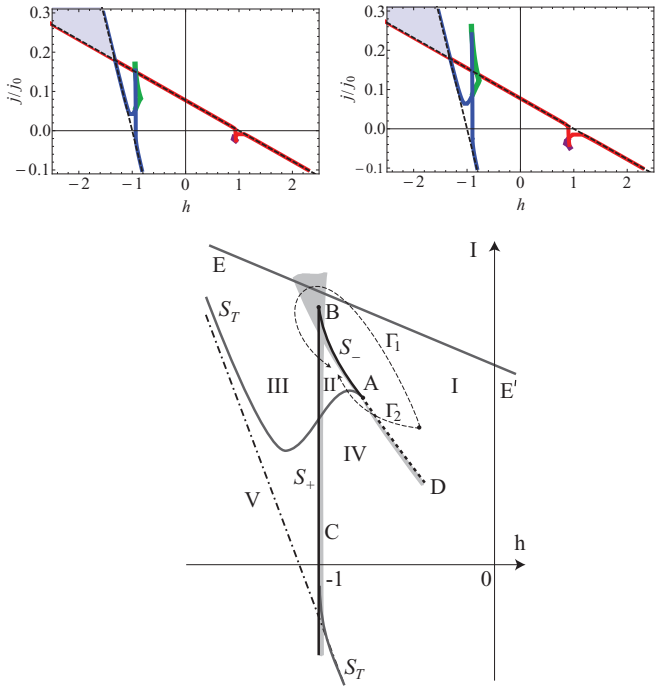

FIG. 8. (Color online) Switching diagram for a misaligned field. (Upper panel) Calculation for the tilt angle $\tan\beta = 0.01$ (left) and $\tan\beta = 0.02$ (right). The dashed lines show the $\beta = 0$ critical curves. (Lower panel) Sketch (drawn not to scale) of the features produced by the field misalignment. The regions and special points are marked as in Fig. 5: The $S_{\rm T}$ curves are dark gray, the $S_{\pm}$ curves are black, the light gray bands contain the node-type equilibria, etc. The dash-dotted straight line represents the $S_{\rm T}$ curve in the $\beta = 0$ case.

We can now discuss the (h, j) switching diagrams in a misaligned field. The critical curves in the (h, j) plane can be obtained as follows. For each value of current the Γ_β line intersects the critical surface at a field $\tilde{h}$ which can be found from a system of equations,

$$h_{c\perp}(\theta, j) = \tilde{h}\sin\beta, \quad h_{cz}(\theta, j) = \tilde{h}\cos\beta.$$

Solving this system for the unknowns θ, $\tilde{h}$ one finds the expression for the critical curve $\tilde{h}(j,\beta)$ in the (h, j) plane. This procedure was performed numerically using the results of Sec. III for $h_{c\perp}(\theta, j)$ and $h_{cz}(\theta, j)$. The resulting plots are shown in Fig. 8, where the upper panels show the typical results of calculations, and the lower panel sketches the features of the critical curves produced by the field misalignment. The $S_{\rm T}$ boundary, which was a straight line at $\beta = 0$ (dash-dotted line), is separated into two curved pieces: one above and one below the h axis. The pieces AB and BC of the $S_{\pm}$ boundary become relevant and serve as a connection between the pieces of $S_{\rm T}$. The larger the tilt angle β of the applied field, the higher point B rises above the zero-tilt $S_{\rm T}$ boundary. Eventually B can rise above the stability boundary EE' of the $\mathbf{m}^{(-)}_{\rm min}$ equilibrium, a situation which actually occurs for the parameters used in the upper panels. The critical curves divide the (h, j) plane into the regions that correspond to the regions shown in Fig. 5 and are numbered in the same way. Transitions between those regions follow the pattern described in Sec. III C. Additionally, the upper panels of Fig. 8 show gray areas where a precessional motion of the free layer occurs.[4,7,18] The method used in this paper does not allow one to study the precession states of a spin-transfer device systematically. For example, it cannot capture the areas where a stable precession coexists with stable static equilibria.[18] The study of precession states in a misaligned field should become a subject of future research.

One important conclusion is that there is no bottleneck phenomenon in the (h, j) switching diagram. Starting from a stable minimum in region I or IV it is possible to get into the stable maximum state in region III along any trajectory that goes above point B, and there is no restriction on how high such a trajectory may rise above this point (the EE' line has no relevance to this process). It is true though, that the larger is the value of β, the larger current is needed to go above the point B in the (h, j) plane. The way to understand this result is to note that the width of the astroid bottleneck increases with current, so at higher currents it is possible to make it wide enough to contain the whole Γ_β trajectory.

Our exact (h, j) switching diagrams exhibits some qualitative differences from the results obtained in Le Gall *et al.*[15] by an approximate method. On the one hand, the approximation of small equilibrium displacements used in that paper seems to predict an equivalent of an infinite rise of point B (Figs. 13 and 14 of Ref. 15). On the other hand, their LLG simulations predict finite jumps of the stability boundaries (Fig. 16 of Ref. 15) that are much closer to our results and may differ from them simply due to a limited number of initial conditions used in numeric simulations. In addition, our approach predicts certain hysteresis phenomena that can be tested in experiments. For example, trajectories Γ_1 and Γ_2 going from region I to region II in Fig. 8 (lower panel) will bring the system into different final states, in full analogy with the trajectories discussed in Fig. 5.

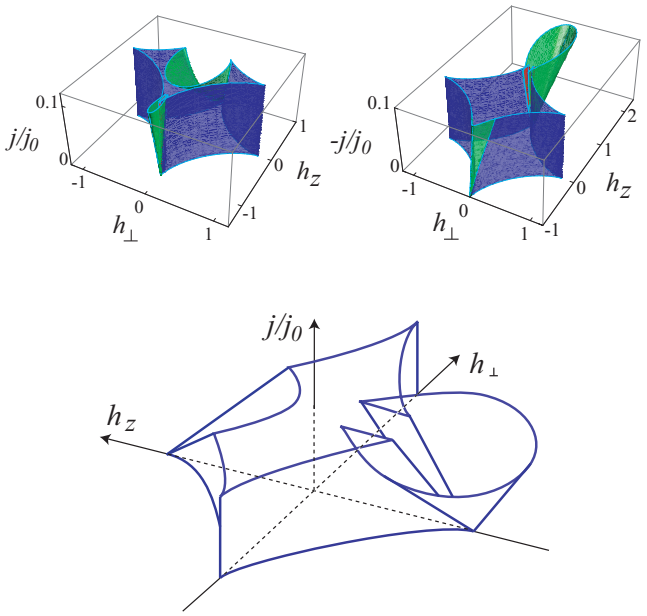

FIG. 9. (Color online) 3D critical surface in the $(h_z, h_\perp, j)$ parameter space. (Upper panel left) Calculation for $j/j_0 > 0$. (Right) $j/j_0 < 0$. The asymmetry of the results is due to the asymmetry of the efficiency factor $g(\cos\theta)$. (Lower panel) A sketch for $j/j_0 > 0$, drawn so as to magnify the features produced by spin torque.

Finally, we present the whole 3D critical surface (Fig. 9). This figure can be obtained by superimposing a sufficient number of fixed current sections found in Sec. III B.

V. CONCLUSIONS

We have calculated the shape of the Stoner-Wholfarth astroid for a uniaxial magnet subject to the spin torque produced by a spin polarizer directed along the easy axis. The shape of the modified astroid can be described as "bubble" connected through a "bottleneck" to the main body of the astroid with a "depression" on the top (Fig 1). Previous calculations[12,15] were improved by using both the trace and the determinant criteria of stability in an exact fashion instead of using an approximation of small equilibrium displacements. Such an approximation cannot be justified whenever some equilibria are already close to each other at zero current, as is the case near the boundary of the conventional astroid. As a result, it became possible to study the structure of the astroid boundary near the bottleneck and its self-crossing was found. This feature turned out to be related to the stabilization of a maximum state inside the bubble and the presence of three stable equilibria inside the triangles formed by the self-crossing.

We further found that the spin torque produces an "inner tube" region on the phase diagram. In this narrow tube enclosing the easy axis the system has only two equilibrium states and exhibits the same phase portrait and qualitative behavior as when the magnetic field is exactly aligned with the symmetry axis.

Part of the inner tube forms a bottleneck. The narrowness of the bottleneck makes it hard to steer the equilibrium into the lower bubble and observe a stable maximum state, unless one takes special care to limit the deviations of the field from the easy axis. Such deviations naturally occur in real experiments due to the impossibility of a perfect field alignment and this brings up the question of a switching diagram in a misaligned field. We show that at high currents such a diagram looks qualitatively similar to the case of perfect field alignment. This is explained by the effect of bottleneck widening at higher currents. The latter effect also makes it possible to use a variable current setup to circumvent the difficulties of reaching the stable maximum state. Close to zero current any misalignment qualitatively changes the (H,I) switching diagram. The distortions become more prominent and reach larger current magnitudes as the misalignment angle increases. The diagrams calculated in this paper improve the results of Ref. 15 in terms of finding the exact shape of these features and providing an accurate description of the switching pattern created by their presence. While it is still difficult to use the existing experimental results[5,12,15] to distinguish between the exact and the approximate predictions, we suggest how this can be done by studying the hysteretic behavior of the system.

ACKNOWLEDGMENTS

This research was supported by National Science Foundation Grant No. DMR-0847159.

APPENDIX A: QUASIMINIMA AND QUASIMAXIMA IN THE PRESENCE OF SPIN TORQUE

The LLG Eq. (3) has a form $\dot{\mathbf{M}} = \mathbf{F}(\mathbf{m})$, where $\mathbf{F}$ is the torque field. At the equilibrium points, where $\mathbf{F}(\mathbf{m}_0) = 0$, it can be linearized giving the system (13). Depending on the eigenvalues of the matrix $\mathbf{D}$ in the linearized equations the equilibria can be the following: Foci (complex eigenvalues), nodes (real eigenvalues of the same sign), and saddle points (real eigenvalues of the opposite sign). The foci and the nodes can be either stable or unstable, and the saddles are always unstable.

When $I = 0$ and $\alpha = 0$, the minima and the maxima are both foci. The difference between them is the direction of rotation of the field $\mathbf{F}$ around the equilibrium point. We will define the sense of rotation as it is observed by looking from the outside of the unit sphere. Then the minima are the foci with counterclockwise (CCW) rotation and the maxima are the foci with clockwise rotation (CW). Based on this, in the $I \neq 0$ case we call the foci with a CCW rotation the "quasiminima", and the foci with a CW rotation the "quasimaxima." The following table of identification follows.

$I \neq 0, \alpha > 0$	$I = 0, \alpha = 0$
Focus with CCW rotation	Energy minimum
Focus with CW rotation	Energy maximum
Node	–
Saddle	Saddle point of energy

The nodes are the only equilibria that do not have a counterpart among the $I = 0, \alpha = 0$ equilibria.

When $I = 0, \alpha > 0$ the minima are always stable and the maxima are always unstable. In the $I \neq 0, \alpha > 0$ case this one-to-one correspondence between stability and the sense of rotation breaks down. The LLG equation may, for example, exhibit an unstable CCW focus, which should be understood as quasiminimum destabilized by the spin torque.

The sense of rotation is a discrete characteristic, and a given focus remains either CW or CCW when the external parameters, such as magnetic field and current, are gradually changed. In order to change its sense or rotation, a focus must be first transformed into a node. The latter is characterized by the real eigenvalues of $\mathbf{D}$, and the field $\mathbf{F}$ does not have a definite sense of rotation near it.

APPENDIX B: GRAPHIC SOLUTION METHOD

A straightforward way to solve the system (24) would be to express $\sin\phi = h_{st}(\theta)/h_x$ from the second equation and reduce it to one equation on θ. However, we choose to proceed in a little bit different way, which will give us a benefit of being able to simultaneously find the solution and check its stability. The field $\mathbf{h}$ and the equilibrium $\mathbf{m}_0$ are always related to each other through Eq. (12) with a certain value of λ. Solving for λ one gets

$$\lambda = \mathbf{m}_0 \cdot \mathbf{h} = h_x \sin\theta\cos\phi + h_z \cos\theta. \tag{B1}$$

Using Eq. (24) one can now express the right-hand side of this identity in two different ways. From the first equation one gets

$$h_x \cos\phi = \sin\theta + h_z \frac{\sin\theta}{\cos\theta},$$

while from the second

$$h_x \cos\phi = \pm\sqrt{h_x^2 - h_{st}^2(\cos\theta)},$$

where a plus sign is used when $\phi \in [-\pi/2,\pi/2]$ and a minus sign is used when $\phi \in [\pi/2,3\pi/2]$, i.e., the two cases correspond to positive and negative projections m_{0x}. Substituting these relationships into the expression (B1) we find two independent expressions for λ:

$$\lambda = \sin^2\theta + \frac{h_z}{\cos\theta}, \quad \lambda = \pm\sqrt{h_x^2 - h_{st}^2(\cos\theta)} + h_z\cos\theta.$$

The right-hand side of the second equation can be replaced by an expression that does not contain h_z. This is done using a relationship following from (24):

$$h_z = \frac{h_x\cos\phi\cos\theta - \sin\theta\cos\theta}{\sin\theta} = \pm\sqrt{h_x^2 - h_{st}^2(\cos\theta)}\,\frac{\cos\theta}{\sin\theta} - \cos\theta.$$

We finally get

$$\lambda = \sin^2\theta + \frac{h_z}{\cos\theta} \equiv \Lambda_z(\theta), \qquad \lambda = \pm\frac{\sqrt{h_x^2 - h_{st}^2(\cos\theta)}}{\sin\theta} - \cos^2\theta \equiv \Lambda_\pm(\theta). \tag{B2}$$

System (B2) should be understood as follows. For a given field $\mathbf{h} = (h_x,0,h_z)$ all equilibrium angles θ_i are found from the equations,

$$\Lambda_z(\theta) = \Lambda_\pm(\theta). \tag{B3}$$

This transcendental equation involving elementary trigonometric functions can be easily studied numerically.

The value of λ corresponding to a given equilibrium is given by either of the two functions (B2). The latter property allows us to set up a convenient graphic procedure for finding a solution and at the same time checking its stability. We plot

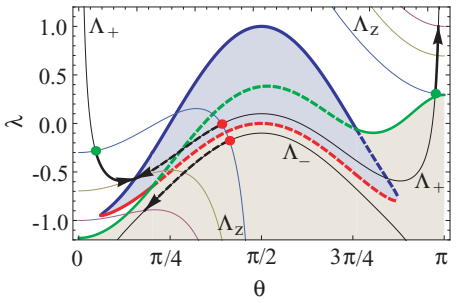

FIG. 10. (Color online) Graphic procedure employed to study the equilibrium states and their stability. Thin solid curves show a family of $\Lambda_c(\theta)$ functions drawn for three values of magnetic field with the same h_x and different h_z projections. Since $\Lambda_\pm$ are h_z independent, the family consists of one Λ_+ curve, one Λ_- curve, and three Λ_z curves. Intersections of these curves give the equilibrium points. The arrows show the evolution of the equilibria with varying external field.

the functions $\Lambda_z(\theta)$, $\Lambda_\pm(\theta)$ and $\lambda_\pm(\theta)$, $\lambda_T(\theta)$ [(18) and (19)] on the same graph (Fig. 10). The horizontal coordinates of the intersections of the $\Lambda_z(\theta)$ and $\Lambda_\pm(\theta)$ curves provide the positions θ_i of all equilibria. The vertical coordinate of each intersection point gives the value of λ corresponding to this equilibrium. If an intersection point lands in the region of stability determined by the criteria (20) or (21), i.e., in the white region in Fig. 10, the equilibrium is stable. As one changes $\mathbf{h}$, the curves $\Lambda_z(\theta)$ and $\Lambda_\pm(\theta)$ are continuously modified, the intersection points move and can enter or leave the region of stability.

A note should be made about the cusp point B of the $S_\pm$ boundary in Figs. 5, 6, etc. We find that this is not the point where S_+ and S_- join each other. An examination of the representative cases leads to conjecture that B is determined by the field $\mathbf{h}$ at which the functions $\lambda_-(\theta)$ and $\Lambda_\pm(\theta,\mathbf{h})$ touch each other. This is consistent with the fact that a saddle point collides with the quasiminimum on the BC and with a quasimaximum on the BAD curves.

*syan@physics.sc.edu
†Current address: Department of Electrical and Computer Engineering, UCSD, La Jolla, CA 92093.
‡yar@physics.sc.edu

[1] A. Hubert and R. Schafer, *Magnetic Domains: The Analysis of Magnetic Microstructures* (Springer, New York, 2008).
[2] E. C. Stoner and E. P. Wohlfarth, Philos. Trans. R. Soc. London A **240**, 599 (1948); J. C. Slonczewski, IBM Research Memorandum No. 003.111.224 (1956); L. D. Landau and E. M. Lifshitz, in *Electrodynamics of Continuous Media* (Pergamon, New York, 1960), Sec. 37.
[3] L. Berger, J. Appl. Phys. **49**, 2156 (1978); Phys. Rev. B **33**, 1572 (1986); **54**, 9353 (1996).
[4] J. C. Slonczewski, J. Magn. Magn. Mater. **159**, L1 (1996).
[5] S. Mangin, D. Revelosona, J. A. Katine, M. J. Carey, B. D. Terris, and E. Fullerton, Nat. Mater. **5**, 210 (2006).
[6] J. Z. Sun, J. Magn. Magn. Mater. **202**, 157 (1999).
[7] Ya. B. Bazaliy, B. A. Jones, and S.-C. Zhang, J. Appl. Phys. **89**, 6793 (2001); arXiv:cond-mat/0009034.
[8] J. A. Katine, F. J. Albert, R. A. Buhrman, E. B. Myers, and D. C. Ralph, Phys. Rev. Lett. **84**, 3149 (2000).
[9] J. C. Slonczewski, J. Magn. Magn. Mater. **247**, 324 (2002).
[10] J. Z. Sun, Phys. Rev. B **62**, 570 (2000).
[11] S. Mangin, Y. Henry, D. Ravelosona, J. A. Katine, and E. E. Fullerton, Appl. Phys. Lett. **94**, 012502 (2009).
[12] Y. Henry, S. Mangin, J. Cucchiara, J. A. Katine, and E. E. Fullerton, Phys. Rev. B **79**, 214422 (2009).
[13] W. Lin, J. Cucchiara, C. Berthelot, T. Hauet, Y. Henry, J. A. Katine, E. E. Fullerton, and S. Mangin, Appl. Phys. Lett. **96**, 252503 (2010).
[14] J. Cucchiara, E. E. Fullerton, A. D. Kent, J. Z. Sun, Y. Henry, and S. Mangin, Phys. Rev. B **84**, 100405(R) (2011).
[15] S. Le Gall, J. Cucchiara, M. Gottwald, C. Berthelot, C.-H. Lambert, Y. Henry, D. Bedau, D. B. Gopman, H. Liu, A. D. Kent, J. Z. Sun,

W. Lin, D. Ravelosona, J. A. Katine, E. E. Fullerton, and S. Mangin, Phys. Rev. B **86**, 014419 (2012).
[16]J. H. Chang, H. H. Chen, and C. R. Chang, Phys. Rev. B **83**, 054425 (2011).
[17]E. Oniciuc, L. Stoleriu, and A. Stancu, Spin **2**, 1250003 (2012).
[18]Ya. B. Bazaliy, B. A. Jones, and S. C. Zhang, Phys. Rev. B **69**, 094421 (2004).
[19]M. D. Stiles and A. Zangwill, Phys. Rev. B **66**, 014407 (2002).
[20]K. Xia, P. J. Kelly, G. E. W. Bauer, A. Brataas, and I. Turek, Phys. Rev. B **65**, 220401(R) (2002).
[21]Y. Tserkovnyak, A. Brataas, G. E. W. Bauer, and B. I. Halperin, Rev. Mod. Phys. **77**, 1375 (2005).
[22]D. C. Ralph and M. D. Stiles, J. Magn. Magn. Mater. **320**, 1190 (2008).
[23]A. Thiaville, Phys. Rev. B **61**, 12221 (2000).
[24]N. Smith, J. A. Katine, J. R. Childress, and M. J. Carey, IEEE Trans. Magn. **41**, 2935 (2005).
[25]I. Sodemann and Ya. B. Bazaliy, Phys. Rev. B. **84**, 064422 (2011).
[26]Z. Li and S. Zhang, Phys. Rev. B **69**, 134416 (2004).
[27]C. Serpico, J. Magn. Magn. Mater. **290-291**, 48 (2005).
[28]C. Serpico, M. d'Aquino, G. Bertotti, and I. D. Mayergoyz, J. Magn. Magn. Mater. **290-291**, 502 (2005).
[29]Z. Li, J. He, and S. Zhang, Phys. Rev. B **72**, 212411 (2005).
[30]D. M. Apalkov and P. B. Visscher, Phys. Rev. B **72**, 180405(R) (2005).
[31]C. Serpico, R. Bonin, G. Bertotti, I. D. Mayergoyz, and M. dAquino, IEEE Trans. Magn. **42**, 2679 (2006).